

Relationship Between Designed Three-Dimensional YSZ Electrolyte Surface Area and Performance of Solution-Precursor Plasma-Sprayed $\text{La}_{0.8}\text{Sr}_{0.2}\text{MnO}_{3-\delta}$ Cathodes

Shan-Lin Zhang, Jiang-Yuan Huang, Cheng-Xin Li, Guan-Jun Yang, and Chang-Jiu Li

(Submitted July 23, 2016; in revised form September 20, 2016)

Active three-phase boundaries (TPBs) significantly influence cathode performance in solid oxide fuel cells, but obtaining long TPBs and understanding the mechanism underlying the improved cathode performance when the electrolyte is prepared with a smooth surface by a high-temperature sintering process remain essential challenges. In this work, we used flame spraying to deposit single-layer semimolten particles on a smooth electrolyte to build a three-dimensional surface with enlarged active surface area and thus increased TPBs. Meanwhile, $\text{La}_{0.8}\text{Sr}_{0.2}\text{MnO}_{3-\delta}$ (LSM) cathodes with fine microstructure were deposited by solution-precursor plasma spraying (SPPS) on the designed electrolyte to establish a three-dimensional cathode–electrolyte interface. The deposition behavior of the semimolten particles on the smooth electrolyte and LSM cathodes on the three-dimensional electrolyte surface was studied. The effects of the area enlargement factor (α_{area}) on the polarization resistance of the SPPS LSM cathodes were investigated, using three-dimensional electrolytes with α_{area} from 1.29 to 2.48. The results indicated that convex particles with different molten states bonded well with the electrolytes. SPPS LSM cathodes also showed good interfacial bonding with convex particles. Finally, the cathode polarization (R_p) decreased linearly with increase of α_{area} . At 800 °C, R_p decreased from 0.98 to 0.32 $\Omega \text{ cm}^2$ when α_{area} was increased from 1.29 to 2.48.

Keywords cathode, solid oxide fuel cells (SOFCs), thermal spraying, three-dimensional electrolyte, three-phase boundaries (TPBs)

1. Introduction

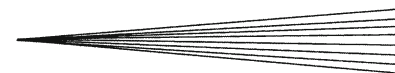
Solid oxide fuel cells (SOFCs) can convert chemical energy stored in a fuel to electricity, exhibiting advantages such as fuel flexibility, high efficiency, low emissions, and environmental friendliness (Ref 1-4). Nowadays, most preparation methods for SOFCs are based on high-temperature sintering after processes such as screen printing (Ref 5), tape casting (Ref 6, 7), dip coating (Ref 8), etc.; For example, fabrication of a dense yttria-stabilized zirconia (YSZ) electrolyte membrane usually requires sintering at temperature >1200 °C (Ref 9). During this high-temperature sintering process, the electrolyte surface tends to become smooth. It is known that the electrolyte

surface condition has significant effects on cathode performance, which is mainly determined by the length of three-phase boundaries (TPBs), especially when pure electronic materials are applied as the cathode. A smooth electrolyte surface provides the smallest effective area for TPB formation. Although use of a composite cathode can increase cathode performance by increasing the TPB length, the most widespread methods for fabrication of composite cathodes adopt either a screen-printing or infiltration approach (Ref 10-12), being tedious and requiring many steps to achieve a desired mass loading. Therefore, determining how to improve the electrolyte surface condition is very important for high-temperature sintering of SOFCs.

As we reported in recent years (Ref 13-15), flame-sprayed semimolten particles can be applied to prepare high-porosity coatings and deposits for use as abradable sealing coatings (Ref 16) or to prepare composite materials. Herbstritt et al. (Ref 17) reported that sintered individual particles prepared by screen printing on a smooth electrolyte surface can also increase the electrochemically active area. Therefore, based on the characteristics of semimolten deposition and convex particle design, we proposed a method to build three-dimensional electrolyte surfaces to address the problem mentioned above. In this design, single-layer semimolten particles are deposited on a smooth electrolyte surface. The convex particles significantly increase the specific surface area and thus increase the active sites (TPB length) for cathodic

Shan-Lin Zhang and Jiang-Yuan Huang contributed equally to this work.

Shan-Lin Zhang, Jiang-Yuan Huang, Cheng-Xin Li, Guan-Jun Yang, and Chang-Jiu Li, State Key Laboratory for Mechanical Behavior of Materials, School of Materials Science and Engineering, Xi'an Jiaotong University, Xi'an 710049, Shaanxi, China. Contact e-mail: licx@mail.xjtu.edu.cn.



reactions. In previous studies (Ref 18, 19), we found that such a structured electrolyte can obviously improve the cathode performance. However, in those studies, the relationship between electrolyte condition and cathode performance was not investigated quantitatively. Firstly, the influence of the structured electrolyte surface on cathode performance should be clarified. Besides, the cathode should use common materials and be prepared by a conventional method.

In this study, we used flame spraying to deposit single-layer semimolten particles on a smooth electrolyte. There were several reasons for choosing flame spraying instead of plasma spraying to build the three-dimensional electrolyte surface. Firstly, the melting degree can be easily controlled because of the relatively low flame temperature, whereas in plasma spraying, most particles are heated to fully molten state due to the rather high plasma temperature ($>10,000$ K). Secondly, powders can be easily injected into the flame center in axial direction (as almost all flame spray torches are designed for axial injection). Therefore, a uniform heating and acceleration process can easily be achieved. Finally, the velocity of the particles is relatively low because of the lower flame velocity compared with other thermal spray process, such as plasma spraying. At high particle velocity, splashing of the molten phase always occurs and the solid core tends to bounce during impact. By controlling the particle coverage rate, different enlarged three-dimensional electrolyte surfaces were formed. The deposition behavior of the semimolten particles was studied, and the relationship between the area enlargement factor and the convex particles was determined.

Meanwhile, solution-precursor plasma spraying (SPPS) was used to deposit porous cathodes, because this process has the ability to fabricate nanostructures, which are critical for increasing TPBs. The deposition behavior of the SPPS LSM cathodes on the convex particles was investigated. In the present study, thermal spraying (TS) was developed as a cost-effective fabrication process, since it has been proven to be a low-cost, time-saving, large-scale industrial production process that does not require a high-temperature sintering process (Ref 20). As-sprayed electrodes and electrolytes can be directly used for SOFCs without any additional procedures such as high-temperature sintering. Besides, the thermal spraying process is suitable for metal-supported SOFCs and other cells with complex geometry. Moreover, its high manufacturing efficiency can shorten the time required for cell fabrication. In our previous studies, both dense electrolyte membranes (Ref 21, 22) and porous electrode layers (Ref 23-25) were successfully produced using a TS process. Here, $\text{La}_{0.8}\text{Sr}_{0.2}\text{MnO}_3$ (LSM) was used as the cathode material, because it is the material closest to commercialization. Moreover, LSM exhibits excellent stability with YSZ, the most popular electrolyte material. Most importantly, LSM is a pure electronic conductor. Therefore, the relationship between the electrolyte surface area and the cathode performance can be investigated, because the latter is mainly determined by the TPB length.

2. Experimental

2.1 Three-Dimensional Electrolyte Surface Formation

A conventional flame spraying system (QH2000, Shanghai) was used to build three-dimensional electrolyte surfaces. Both commercially available agglomerated powders and fused-crushed powders can be used to obtain semimolten particles, but to control the melting degree and investigate the relationship between particle size and melting behavior, dense spherical YSZ particles with narrow size distribution are needed. Therefore, commercially available fused-crushed 8YSZ powder (Fujimi Co., Japan) with size range of 5 to 25 μm was spheroidized by flame spraying first. After emerging from the flame jet, the powder particles were collected using water, then graded by plain sedimentation in water. Spherical powder with size range of 10 to 15 μm was chosen for spraying to build the three-dimensional electrolyte surface. Figure 1 shows the morphology of the resulting spherical powder. It can be seen that the powder had a smooth surface and narrow size distribution.

Polished YSZ pellets with diameter of 20 mm and thickness of 1 mm were used as electrolyte substrates. Flame-sprayed semimolten particles were deposited on the electrolyte surface using the spherical YSZ powder. Acetylene (C_2H_2 , 5 slpm) and oxygen (O_2 , ~ 20 slpm) gases were supplied to generate the flame. The powders were injected into the flame from the central inlet using oxygen as carrier gas. The powder feed rate was controlled at ~ 10 g/min. To obtain particles in semimolten state, individual particles were deposited at spray distance of 20 mm. Before spraying, the substrate was heated to slightly higher than 600 $^\circ\text{C}$ by the flame to achieve good bonding between the substrate and semimolten particles. The surface coverage fraction (or surface enlargement) was controlled by adjusting the number of torch scanning passes (from three to seven). During spraying, the flame torch was manipulated using a robot at speed of 0.5 m/s.

2.2 Spraying Parameters for Solution-Precursor Plasma Spraying of LSM Cathode

Stoichiometric amounts of $\text{La}(\text{NO}_3)_3 \cdot 6\text{H}_2\text{O}$ (99.99%, SCRC), $\text{Sr}(\text{NO}_3)_2 \cdot 6\text{H}_2\text{O}$ (99.99%, SCRC), and 50% $\text{Mn}(\text{NO}_3)_2$ solution (99.9%, SCRC) were dissolved in water/alcohol (99.7%, Ante) solvent (1:3 vol.%) to obtain nitrate solution with total cationic concentration of 0.2 mol/L. The prepared solution was sprayed using a conventional air plasma spraying system (GDP-80, Jiujiang, China). The precursor solution was injected into the plasma jet at feed rate of 150 mL/min using a peristaltic pump. LSM cathode layers were deposited on an area of 0.5 cm^2 with thickness of 15 to 20 μm at plasma arc power of 30 kW. The primary gas Ar and secondary gas H_2 pressures were fixed at 0.8 and 0.4 MPa, respectively. The flow rates of Ar and H_2 were set to 40 and 3 L/min, respectively. The spray distance was maintained at 60 mm. During spraying, the plasma torch was manipulated by a

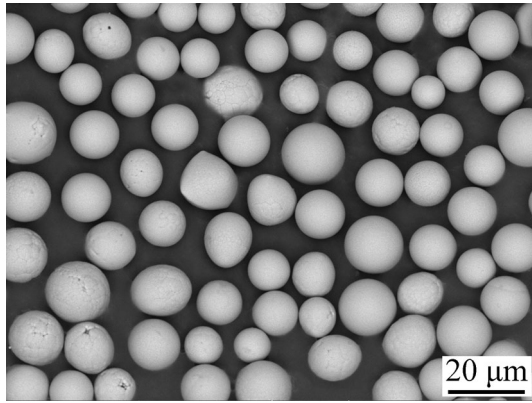


Fig. 1 Surface morphology of spherical YSZ powder

robot at speed of 0.5 m/s. The cathode thickness was controlled by the number of torch scanning passes. In this study, all samples were deposited using two passes.

2.3 Characterization

The surface morphology and microstructure of the convex-structured electrolyte surface and cathodes were analyzed by scanning electron microscopy (SEM, TESCAN MIRA 3 LMH, Czech Republic). The phase composition of the prepared cathodes was characterized by x-ray diffraction (XRD) analysis (X'Pert PRO, PANalytical, The Netherlands). Three-dimensional confocal laser scanning microscopy (CLSM) was employed to measure the melting degree (M) of single particles and the area enlargement factor (α_{area}) for the convex-structured electrolyte surface. The melting degree of single semimolten particles can be calculated as follows:

$$M = (D - d)/D, \quad (\text{Eq 1})$$

where D is the original particle diameter and d is the diameter of the nonmolten core.

First, the volume of a single deposit was measured by three-dimensional confocal laser scanning microscopy. Since the original particles were spherical, D can be calculated from their volume. According to our previous study (Ref 14), the diameter of the nonmolten core is equal to the height of the deposit center, which can also be measured by three-dimensional CLSM. Finally, the melting degree of a single particle was obtained using Eq 1.

The area enlargement factor can be calculated as follows:

$$\alpha_{\text{area}} = \sum A_{\text{surf}} / \sum A_{\text{pro}}, \quad (\text{Eq 2})$$

where A_{surf} is the surface area of a single particle and $\sum A_{\text{surf}}$ is the total surface area of deposited particles over the apparent surface area of the substrate A_{pro} . Moreover, the surface coverage ratio was defined as the ratio between the total A_{pro} and the total area. In the present study, for the single particles with similar diameter, at least 20 individual particles were measured to obtain the

average melting degree and single area enlargement factor ($\alpha_{\text{area-p}}$). For the total area enlargement factors ($\alpha_{\text{area-t}}$), at least five regions from each of three samples were measured.

To characterize cathode performance, Pt pastes were attached as the counterelectrode and reference electrode to form LSM/YSZ/Pt cells. The distance between the Pt reference electrode and LSM working electrode was about 4 mm. Prior to electrochemical characterization, Pt paste/meshes were also attached onto the LSM cathode and annealed at 800 °C in air for 2 h to act as current collectors. Electrochemical impedance spectroscopy (EIS) of the cells was then carried out using a Solartron SI 1260/1287 impedance analyzer in ambient air under open-circuit voltage (OCV) conditions. The sweeping frequency range was 0.1 Hz to 10^5 Hz at alternating-current (AC) voltage amplitude of 20 mV. The three-electrode configuration and test approach were used, as applied elsewhere (Ref 26).

3. Results and Discussion

3.1 Deposition Behavior and Microstructure of Semimolten YSZ Particles for Forming Three-Dimensional Electrolyte Surfaces

Figure 2(a), (c), and (e) show typical surface morphologies of the convex-structured electrolyte with different particle surface coverage ratios. Figure 2(b), (d), and (f) show 3D CLSM images of the surface morphologies of electrolytes with different particle surface coverage ratios. Firstly, it can be seen that all the particles deposited on the electrolyte surface exhibited semimolten state. Furthermore, the surface coverage ratio could be varied from 38 to 87% by controlling the number of scanning passes. In the present study, five groups of samples with surface coverage ratio of 38% (three passes), 49% (four passes), 60% (five passes), 70% (six passes), and 87% (seven passes), respectively, were prepared. Finally, according to their 3D shapes, it was observed that the deposited particles showed different melting states even through the spray particles had a narrow size distribution. As mentioned above, it can be concluded that three-dimensional electrolyte surfaces can be successfully prepared by flame spraying with semimolten particles.

Figure 3 shows typical cross-sectional views of single particles with different melting degrees. It can be seen that particles with both high (Fig. 3a) and low (Fig. 3b) melting degrees bonded well with the electrolyte substrate. After impact of the semimolten particles on the substrate, the molten fraction of the particle surface will flow to the contact region between the solid core and substrate owing to the inertia of the impacting particle. Then, after solidification of the melt, the nonmolten solid core was joined to the substrate and welded by the melt through chemical interfacial bonding. Good interfacial bonding between the particles and bulk electrolyte allowed oxygen ions to transfer rapidly across the interface to the bulk electrolyte. Therefore, the designed three-dimensional electrolyte

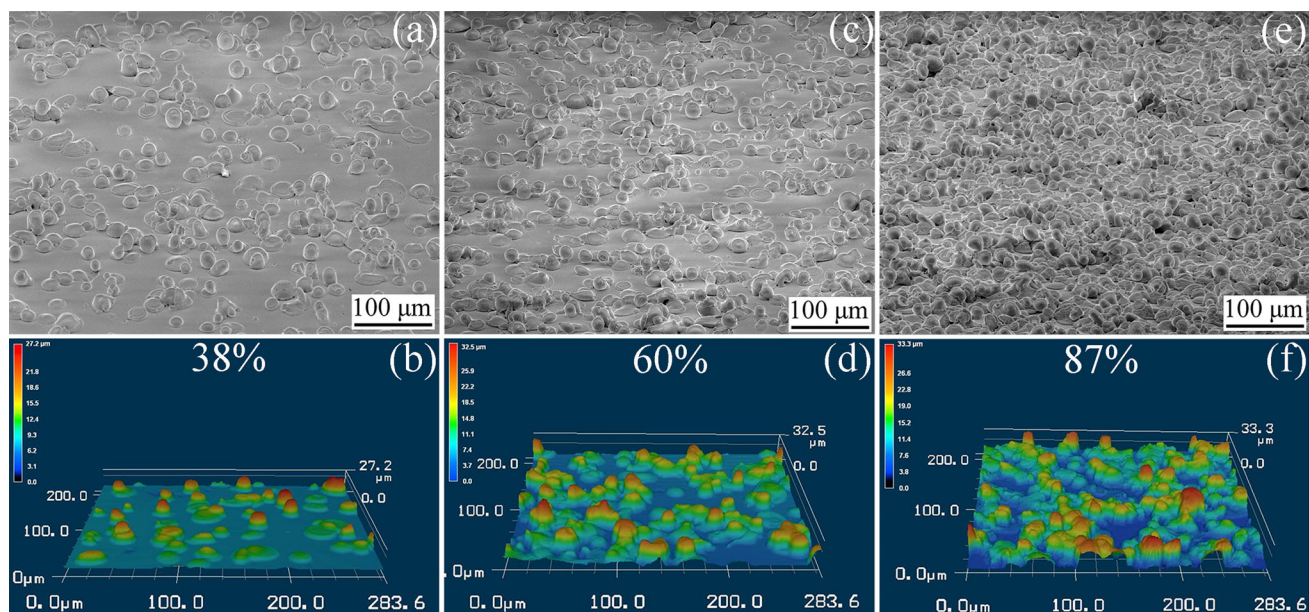


Fig. 2 SEM and 3D confocal laser scanning images of three-dimensional electrolyte surfaces obtained with different surface coverage rates: (a, b) 38%, (c, d) 60%, and (e, f) 87%

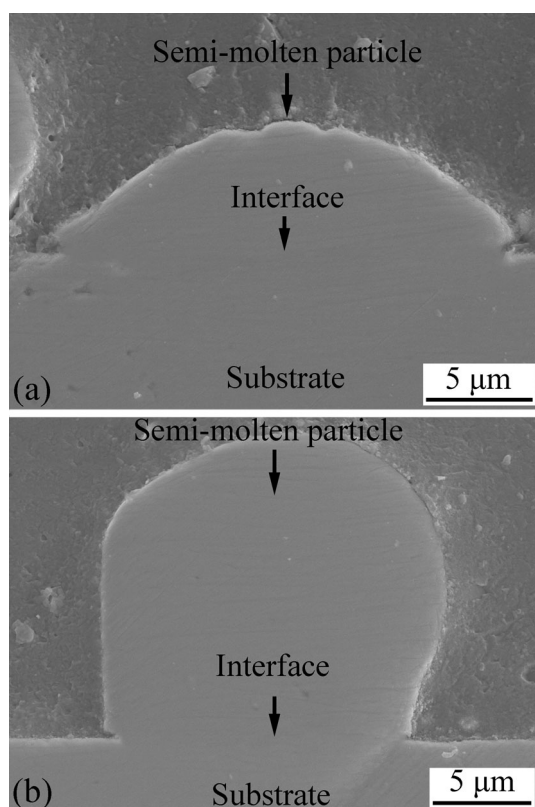


Fig. 3 Cross-sectional views of single particles with (a) high and (b) low melting degree

surfaces can be used to study the effects of the structured surface on cathode performance.

Figure 4(a) shows the relation between the melting degree of an individual particle and its diameter. These results indicate that the melting degree decreased with increasing particle diameter. For particles with diameter of about $12 \mu\text{m}$, the melting degree reached about 60%, while, when the particle diameter increased to about $19 \mu\text{m}$, the melting degree decreased to about 17%. The influence of diameter on the melting degree is consistent with other thermal spray processes, since theoretically, the smaller the spray particle size, the faster the heat transfer from the flame to the particles. Even through the powder particles had a narrow size distribution of about 10 to $20 \mu\text{m}$ in the present study, the sensitivity of the melting degree to the particle diameter led to a variety of morphologies of deposited particles, as shown in Fig. 1. Figure 4(b) shows the effect of particle diameter on the area enlargement factor ($\alpha_{\text{area-p}}$) for individual deposited particles. It was found that $\alpha_{\text{area-p}}$ increased rapidly with increasing particle diameter. In fact, according to Fig. 4(a), it can be concluded that $\alpha_{\text{area-p}}$ was mainly influenced by the melting degree. Simply speaking, if the melting degree is 100%, $\alpha_{\text{area-p}}$ is approximately equal to 1, because the splat would spread well on the flat substrate. On the other hand, if the melting degree is close to zero, $\alpha_{\text{area-p}}$ will be close to 4, because it is just like a spherical particle adhering to the substrate. Figure 4(c) shows the total area enlargement factor ($\alpha_{\text{area-t}}$) for samples with different surface coverage ratios. These results indicate

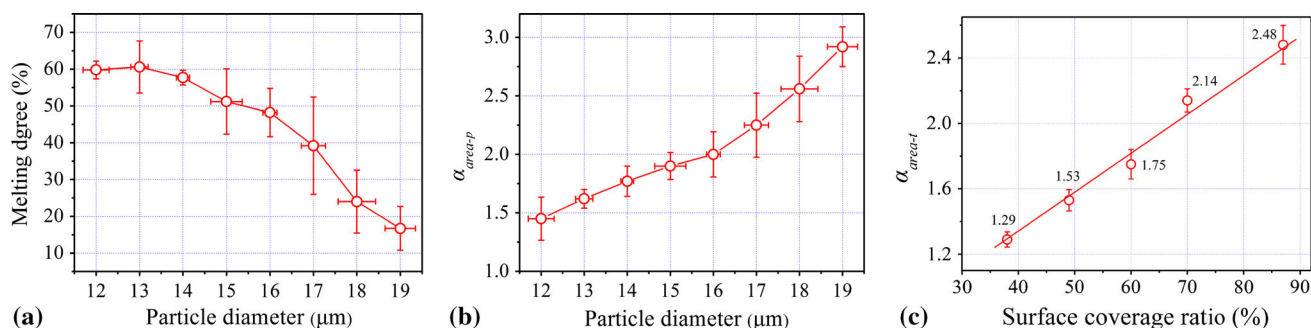


Fig. 4 Effect of particle diameter on (a) melting degree and (b) area enlargement factor of single particles (α_{area-p}), and (c) relationship between surface coverage rate and total area enlargement factor (α_{area-t})

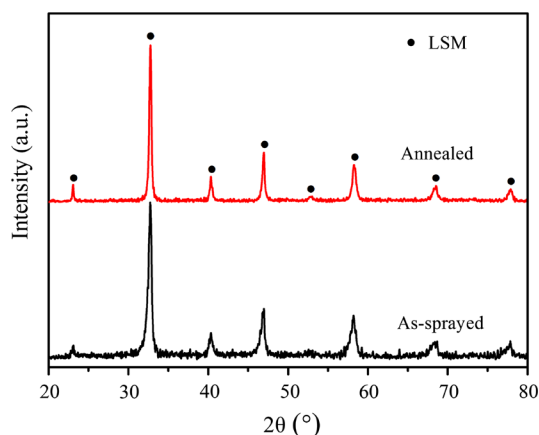


Fig. 5 XRD patterns for SPPS LSM cathodes

that α_{area-t} increased linearly with increasing surface coverage ratio. For the sample with mean surface coverage ratio of ~38%, α_{area-t} was about 1.29. When the mean surface coverage ratio was increased to 87%, α_{area-t} reached about 2.48 in the present study. Therefore, α_{area-t} can indeed be accurately controlled by controlling the surface coverage ratio. According to these results, it can be concluded that flame spraying with semimolten particles onto a flat surface should be an effective method to investigate the effect of the electrolyte surface state on cathode performance.

3.2 Microstructure and Deposition Behavior of Suspension Plasma-Sprayed LSM Cathode on Three-Dimensional Electrolytes

Figure 5 shows the XRD patterns of the as-sprayed and annealed LSM cathodes. Clearly, these XRD patterns are similar to the standard XRD pattern of LaMnO_3 (PDF 053-0058), suggesting single-phase perovskite LSM with a high degree of crystallization. Compared with the as-sprayed LSM deposit, the crystallization increased after annealing at 800 °C for 5 h.

Figure 6(a) shows the typical surface morphologies of the SPS LSM cathode deposited on flat YSZ. As shown in the image at low magnification, the SPS LSM cathode exhibited a rough and porous, island-like morphology. At

higher magnification (inset), it can be seen that the cathode was composed of agglomerates of spherical particles with size of approximately 0.2 to 1 μm. Moreover, the particles were well connected through sintering necks. Figure 6(b) shows the morphology of the cross-section of the cathode deposited on the unmodified electrolyte. This image clearly shows that the cathode had thickness of 10 to 15 μm and was well bonded with the YSZ electrolyte. Moreover, it shows that the SPPS LSM cathode had high porosity and was composed of submicrometer particles. The LSM particles are well connected by sintering-like necks.

To study the deposition behavior of SPPS LSM cathodes on the three-dimensional electrolytes, the microstructure of the interfaces between the LSM cathode and YSZ electrolyte were characterized on a polished cross-section. Figure 7 shows the microstructure of the interfaces between the LSM cathode and semimolten particles with different melting degrees. From Fig. 7(a), it can be seen that the LSM cathode shows porous structure and is bonded well with the YSZ, even though it had a smooth surface. According to the microstructure, the SPPS LSM had porosity of ~30%. Figure 7(b) to (d) show the interfaces (indicated by arrows) between the LSM cathode and deposited YSZ particles having different melting degrees. Similarly to the results for the flat surface, the SPPS LSM cathode was bonded well with the semimolten particles. Moreover, it was seen that the cathode could also be deposited and bonded well to the semimolten particles at the occlude area, as shown in Fig. 6(d), when the particle had low melting degree. For a liquid spraying process, the particle size is smaller than for conventional thermal spraying. Because of their low inertia, the small particles will follow the plasma gas stream toward the occluded region and then deposit. As a result, all of the electrolyte surface can be covered with the cathode without blind areas. Therefore, all of the enlarged surface can be considered effective when studying the effects of the electrolyte surface condition on cathode performance.

3.3 Effect of Electrolyte Surface Structure on Cathode Performance

Figure 8 shows typical impedance data obtained from cells comprising LSM cathodes deposited on electrolytes with different α_{area} values at 800 °C. To easily compare the cathode polarization resistance (R_p), the Ohmic

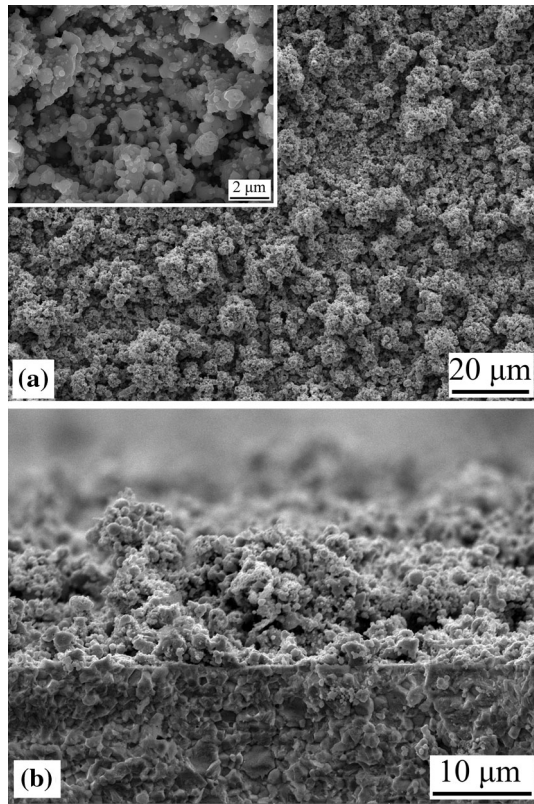
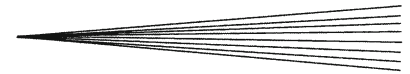


Fig. 6 Morphologies of (a) surface and (b) cross-section of SPPS LSM cathode

resistances (which mainly result from the electrolyte) were removed from the impedance data, because all the electrolytes had the same thickness. The Ohmic resistance can be estimated from these spectra from the intercepts with the abscissa at high frequency. Besides, at high temperature, the left semicircle in the high-frequency region of the spectrum corresponds to the grain-boundary resistance (R_{gb}), which can be attributed to migration of grain boundaries in the YSZ electrolyte (Ref 27, 28); this effect is too small to be distinguished in these spectra because of the high grain-boundary conductivity at high temperature. Therefore, R_p can be obtained from the intercept of the semicircle.

According to the Nyquist plots, the R_p value for different cathodes at different temperatures was obtained and is shown in Fig. 9(a). It can be seen that R_p decreased rapidly with increasing α_{area} . When the LSM cathode was deposited on a polished smooth electrolyte ($\alpha_{area}=1.0$), the cathode exhibited mean R_p of $0.98 \Omega \text{ cm}^2$ at $800 \text{ }^\circ\text{C}$. When the surface was covered by some semimolten particles ($\alpha_{area}=1.29$), R_p decreased to $0.8 \Omega \text{ cm}^2$ at $800 \text{ }^\circ\text{C}$. When α_{area} was further increased to 2.48, the mean R_p decreased to $0.38 \Omega \text{ cm}^2$. These results show that R_p decreased linearly with increasing α_{area} . Besides, the activation energy (E_a) for electrode polarization can be calculated from the linear relationship between $\ln(R_p)$ and $1/T$, as shown in Fig. 9(a), using the Arrhenius law. In the present study, all cathodes had similar E_a values of about

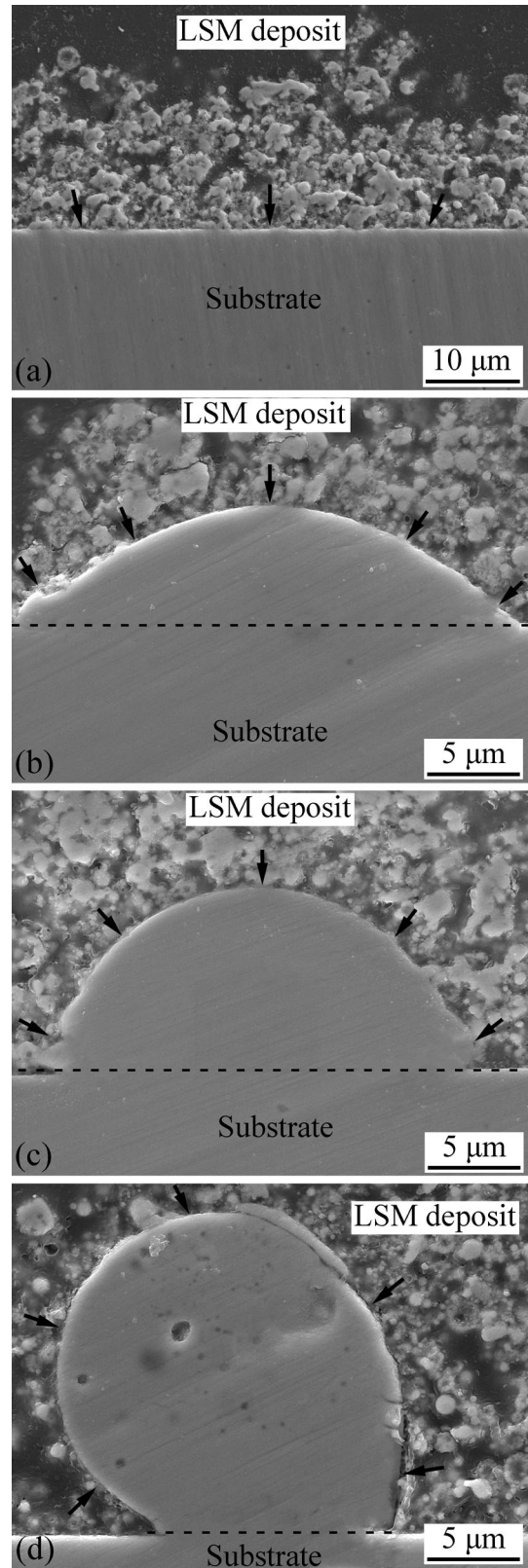


Fig. 7 Microstructure of interface between LSM cathode and semimolten particles on (a) polished electrolyte, and (b), (c), and (d) on semimolten particles with melting degree decreasing in the order: (b) > (c) > (d)

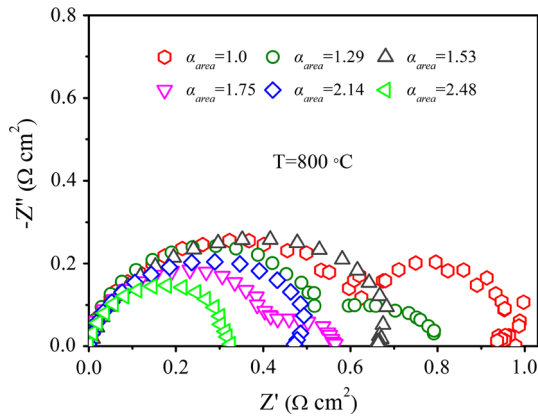


Fig. 8 Nyquist plots for LSM cathodes deposited on different electrolytes at 800 °C

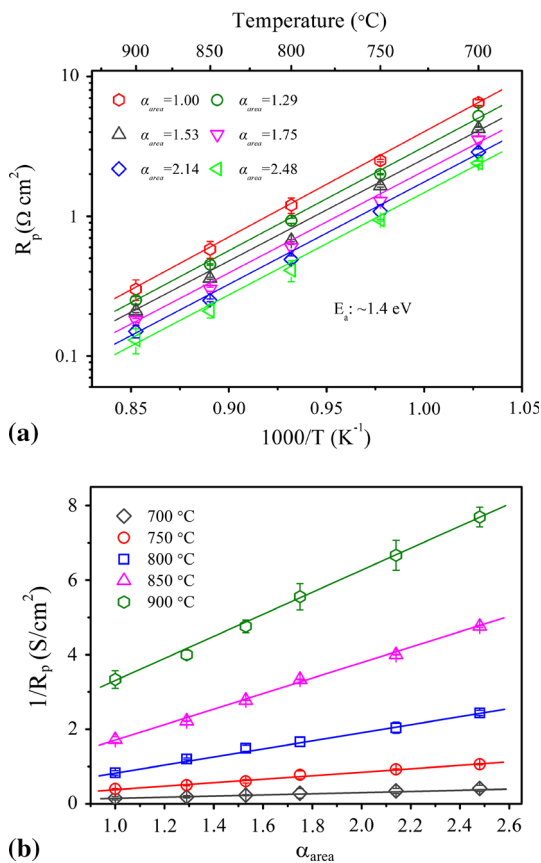


Fig. 9 (a) Arrhenius plots of polarization resistance for cathodes deposited on different electrolytes. (b) α_{area} vs. $1/R_p$ at different temperatures

1.4 eV, similar to results for LSM cathodes reported in literature. This means that the cathode reduction mechanism did not change when the cathode surfaces were covered by semimolten particles.

Figure 9(b) shows the effect of α_{area} on $1/R_p$, indicating the area specific conductivity at different temperatures. It is obviously seen that $1/R_p$ increased linearly with

increasing α_{area} . This also means that the total effective area of the electrolyte surface increased linearly. In other words, the length of TPBs increased linearly with increasing α_{area} .

In fact, LSM is a pure electronic conductor, so the cathode performance is mainly determined by TPBs. Usually, the TPB length per unit area is determined from the cathode porosity and particle size. In the present study, all the cathodes had similar particle size distribution and porosity, because they were all prepared using the same process. Therefore, the TPB length per unit area was the same for each cathode. However, the total surface area of the electrolytes differed, meaning that the total TPB length also varied. With increasing surface area (or α_{area}), the total TPB length also increases. It can be concluded that the total TPB length increased linearly with increasing α_{area} , thus resulting in the linear decrease of R_p . As a result, it can be concluded that deposition of semi-molten particles is an effective method to improve cathode performance, especially when a pure electronic cathode material is used.

4. Conclusions

Deposition of flame-sprayed semimolten particles was applied to construct a three-dimensional electrolyte surface to investigate the effect of such a structured electrolyte surface on cathode performance. Solution-precursor plasma spraying was used to deposit finely structured LSM cathodes on the structured electrolyte. The results indicated that the surface area enlargement factor (α_{area}) could be varied from 1 to 2.48 by adjusting the particle coverage ratio. The semimolten particles bonded well with the electrolyte. Besides, fine cathode particles could be deposited on all of the enlarged surfaces and bonded well with the convex particles. As predicted, the cathode polarization (R_p) decreased linearly with increasing α_{area} . At 800 °C, R_p decreased from 0.98 $\Omega \text{ cm}^2$ to 0.38 $\Omega \text{ cm}^2$ when α_{area} was increased from 1.0 to 2.48.

Acknowledgments

This study was partially supported by the National Basic Research Program (Grant No. 2012CB625100) and China Postdoctoral Science Foundation Grant (No. 2015M580840).

References

1. N.Q. Minh, Ceramic Fuel Cells, *J. Am. Ceram. Soc.*, 1993, **76**, p 563-588
2. S.C. Singhal, Solid Oxide Fuel Cells for Stationary, Mobile, and Military Applications, *Solid State Ion.*, 2002, **152**, p 405-410
3. M. Liu, M.E. Lynch, K. Blinn, F.M. Alamgir, and Y. Choi, Rational SOFC Material Design: New Advances and Tools, *Mater. Today*, 2011, **14**, p 534-546
4. L. Yang, S.Z. Wang, K. Blinn, M.F. Liu, Z. Liu, Z. Cheng, and M.L. Liu, Enhanced Sulfur and Coking Tolerance of a Mixed



- Ion Conductor for SOFCs: BaZr_{0.1}Ce_{0.7}Y_{0.2-x}Yb_xO_{3-δ}, *Science*, 2009, **326**, p 126-129
5. X. Ge, X. Huang, Y. Zhang, Z. Lu, J. Xu, K. Chen, D. Dong, Z. Liu, J. Miao, and W. Su, Screen-Printed Thin YSZ Films Used as Electrolytes for Solid Oxide Fuel Cells, *J. Power Sources*, 2006, **159**(2), p 1048-1050
 6. S. Le, K.N. Sun, N. Zhang, X. Zhu, H. Sun, Y.X. Yuan, and X. Zhou, Fabrication and Evaluation of Anode and Thin Y₂O₃-Stabilized ZrO₂ Film by Co-tape Casting and Co-firing Technique, *J. Power Sources*, 2010, **195**(9), p 2644-2648
 7. F. Dong, Y. Chen, R. Ran, D. Chen, M.O. Tadé, S. Liub, and Z. Shao, BaNb_{0.05}Fe_{0.95}O_{3-δ} as a New Oxygen Reduction Electrocatalyst for Intermediate Temperature Solid Oxide Fuel Cells, *J. Mater. Chem. A*, 2013, **1**, p 9781-9791
 8. H. Tikkanen, C. Suci, I. Wærnhus, and A.C. Hoffmann, Examination of the Co-sintering Process of Thin 8YSZ Films Obtained by Dip-Coating on In-House Produced NiO-YSZ, *J. Eur. Ceram. Soc.*, 2011, **31**(9), p 1733-1739
 9. T. Talebi, M. Haji, and B. Raissi, Effect of Sintering Temperature on the Microstructure, Roughness and Electrochemical Impedance of Electrophoretically Deposited YSZ Electrolyte for SOFCs, *Int. J. Hydrog. Energy*, 2010, **35**(17), p 9420-9426
 10. L. Nie, M. Liu, Y. Zhang, and M. Liu, La_{0.6}Sr_{0.4}Co_{0.2}Fe_{0.8}O_{3-δ} Cathodes Infiltrated with Samarium-Doped Cerium Oxide for Solid Oxide Fuel Cells, *J. Power Sources*, 2010, **195**(15), p 4704-4708
 11. M. Liu, D. Ding, K. Blinn, X. Li, L. Nie, and M. Liu, Enhanced Performance of LSCF Cathode through Surface Modification, *Int. J. Hydrog. Energy*, 2012, **37**(10), p 8613-8620
 12. X. Zhang, H. Zhang, and X. Liu, High Performance La₂NiO_{4+δ}-Infiltrated (La_{0.6}Sr_{0.4})_{0.995}Co_{0.2}Fe_{0.8}O_{3-δ} Cathode for Solid Oxide Fuel Cells, *J. Power Sources*, 2014, **269**, p 412-417
 13. B. Chen, C.-J. Li, G.-J. Yang, J.-T. Yao, H.-B. Huo, and C.-X. Li, Fabrication of Porous Molybdenum by Controlling Spray Particle State, *J. Therm. Spray Technol.*, 2012, **21**(5), p 1032-1045
 14. J.-T. Yao, J.-Q. Ren, H.-B. Huo, G.-J. Yang, C.-X. Li, and C.-J. Li, Deposition Behavior of Semi-molten Spray Particles During Flame Spraying of Porous Metal Alloy, *J. Therm. Spray Technol.*, 2014, **23**(6), p 991-999
 15. J.-T. Yao, C.-J. Li, Y. Li, B. Chen, and H.-B. Huo, Relationships between the Properties and Microstructure of Mo-Cu Composites Prepared by Infiltrating Copper into Flame-Sprayed Porous Mo Skeleton, *Mater. Des.*, 2015, **88**, p 774-780
 16. C.-J. Li, J. Zou, H.-B. Huo, J.-T. Yao, and G.-J. Yang, Microstructure and Properties of Porous Abradable Alumina Coatings Flame-Sprayed with Semi-molten Particles, *J. Therm. Spray Technol.*, 2016, **25**(1), p 264-272
 17. D. Herbstritt, A. Weber, and E. Ivers-Tiffée, Modelling and DC-Polarisation of a Three Dimensional Electrode/Electrolyte Interface, *J. Eur. Ceram. Soc.*, 2001, **21**, p 1813-1816
 18. X.-M. Wang, C.-J. Li, C.-X. Li, and G.-J. Yang, Microstructure and Electrochemical Behavior of a Structured Electrolyte/LSM-Cathode Interface Modified by Flame Spraying for Solid Oxide Fuel Cell Application, *J. Therm. Spray Technol.*, 2010, **19**(1), p 311-316
 19. X.-M. Wang, C.-X. Li, J.-Y. Huang, G.-J. Yang, and C.-J. Li, Deposition Mechanism of Convex YSZ Particles and Effect of Electrolyte/Cathode Interface Structure on Cathode Performance of Solid Oxide Fuel Cell, *Int. J. Hydrog. Energy*, 2014, **39**(25), p 13650-13657
 20. R. Hui, Z. Wang, O. Kesler, L. Rose, J. Jankovic, S. Yick, R. Maric, and D. Ghosh, Thermal Plasma Spraying for SOFCs: Applications, Potential Advantages, and Challenges, *J. Power Sources*, 2007, **170**(2), p 308-323
 21. S.-L. Zhang, C.-X. Li, C.-J. Li, G.-J. Yang, and Z.-H. Han, Scandia-Stabilized Zirconia Electrolyte with Improved Interlamellar Bonding by High-Velocity Plasma Spraying for High Performance Solid Oxide Fuel Cells, *J. Power Sources*, 2013, **232**, p 123-131
 22. S.-L. Zhang, C.-X. Li, and C.-J. Li, Plasma-Sprayed Y₂O₃-Stabilized ZrO₂ Electrolyte with Improved Interlamellar Bonding for Direct Application to Solid Oxide Fuel Cells, *J. Fuel Cell Sci. Technol.*, 2014, **11**, p 031001-031006
 23. C.-X. Li, C.-J. Li, and L.-J. Guo, Performance of a Ni/Al₂O₃ Cermet-Supported Tubular Solid Oxide Fuel Cell Operating with Biomass-Based Syngas through Supercritical Water, *Int. J. Hydrog. Energy*, 2010, **35**(7), p 2904-2908
 24. C.-X. Li, L.-L. Yun, Y. Zhang, C.-J. Li, and L.-J. Guo, Microstructure, Performance and Stability of Ni/Al₂O₃ Cermet-Supported SOFC Operating with Coal-Based Syngas Produced Using Supercritical Water, *Int. J. Hydrog. Energy*, 2012, **37**(17), p 13001-13006
 25. C.-X. Li, C.-J. Li, and L.-J. Guo, Effect of Composition of NiO/YSZ Anode on the Polarization Characteristics of SOFC Fabricated by Atmospheric Plasma Spraying, *Int. J. Hydrog. Energy*, 2010, **35**(7), p 2964-2969
 26. S.C. Singhal and K. Kendall, *High Temperature Solid Oxide Fuel Cells: Fundamentals*, Elsevier, Des. Appl., 2004
 27. N. Ortiz-Vitoriano, A. Hauch, I. Ruiz de Larramendi, C. Bernuy-López, R. Knibbe, and T. Rojo, Electrochemical Characterization of La_{0.6}Ca_{0.4}Fe_{0.8}Ni_{0.2}O_{3-δ} Perovskite Cathode for IT-SOFC, *J. Power Sources*, 2013, **239**, p 196-200
 28. N. Ortiz-Vitoriano, C. Bernuy-López, A. Hauch, I. Ruiz de Larramendi, and T. Rojo, Electrochemical Characterization of La_{0.6}Ca_{0.4}Fe_{0.8}Ni_{0.2}O₃ Cathode on Ce_{0.8}Gd_{0.2}O_{1.9} Electrolyte for IT-SOFC, *Int. J. Hydrog. Energy*, 2014, **39**(12), p 6675-6679